UDC 699.86
DOI: 10.15587/1729-4061.2022.268618

CONSTRUCTION OF A MODEL FOR AN ENCLOSING STRUCTURE WITH A HEAT-ACCUMULATING MATERIAL WITH PHASE TRANSITION TAKING INTO ACCOUNT THE PROCESS OF SOLAR ENERGY ACCUMULATION

Ruslan Kudabayev
Doctoral Student*
Nursultan Mizamov
Doctoral Student
Department of Architecture
South-Kazakhstan Mukhtar Auezov South Kazakhstan University
Tauke Khan str., 5, Shymkent, Republic of Kazakhstan, 160012
Nurlan Zhangabay
Corresponding Author
PhD, Associate Professor**
E-mail: Nurlan.zhanabay777@mail.ru
Ulanbator Suleimenov
Doctor of Technical Sciences, Professor**
Andrii Kostikov
Doctor of Technical Sciences, Professor,
Corresponding Member of the National Academy of Sciences of Ukraine****
Anna Vorontsova
Leading Engineer****
Svetlana Buganova
PhD, Associate Professor
Faculty of Building Technologies, Infrastructure and Management
International Educational Corporation (KazGASA)
Ryskulbekov str., 28, Almaty, Republic of Kazakhstan, 050043
Altynsary Umbitaliyev
Doctor in Economics, Professor
Department of Economics***
Elmira Kalshabekova
PhD, Associate Professor*
Zhumadilla Aldiyarov
PhD, Associate Professor*
*Department of Construction and Construction Materials
Mukhtar Auezov South Kazakhstan University
Tauke Khan str., 5, Shymkent, Republic of Kazakhstan, 160012
Department of Construction*
***Shymkent University
Silk Road str., 150, Karatausky dist., Shymkent, Republic of Kazakhstan, 160031
****Department of Modeling and Identification
of Thermal Processes in Energy Technology Equipment
A. Pidhornyi Institute of Mechanical Engineering Problems
of the National Academy of Sciences of Ukraine
Pozharskogo str., 2/10, Kharkiv, Ukraine, 61046

This paper proposes a mathematical model and a procedure for calculating the thermal state of the enclosing structure of the building, which includes an energy-active panel that accumulates solar radiation due to the phase transition of the heat-accumulating material. The mathematical model is based on a two-dimensional non-stationary nonlinear equation of thermal conductivity, which describes the process of heat transfer in the bearing layer of the enclosing structure and the energy-active panel. The model also includes equations describing radiant heat transfer between opaque and translucent bodies. To correctly describe solar insolation, the ASHRAE 2009 model was used in conjunction with the daily change in the position of the Sun in the sky.

To solve the system of equations that make up the mathematical model, an iterative procedure has been developed, which involves alternating solution at each time step of the two-dimensional equation of thermal conductivity and a set of algebraic equations of convective and radiant heat transfer.

The study's result established that the amount of accumulated energy in the heat-accumulating material of the phase transition during daylight hours increases significantly, from 15 to 35 %. At night, the surface temperature of the heat-accumulating element in structures using a material with a phase transition is greater than in the case of heat accumulation only in the bearing layer. As a result, it is possible to select from 70 to 120 % more accumulated heat while the presence of high-thermal partitions in a heat-accumulating material with a phase transition contributes to an increase in accumulated heat and usable heat

Keywords: enclosing structure, accumulation of solar energy, heat accumulating material, modeling of thermal processes, phase transition

Received date 30.09.2022
Accepted date 02.12.2022
Published date 30.12.2022

How to Cite: *Kudabayev, R., Mizamov, N., Zhangabay, N., Suleimenov, U., Kostikov, A., Vorontsova, A., Buganova, S., Umbitaliyev, A., Kalshabekova, E., Aldiyarov, Z. (2022). Construction of a model for an enclosing structure with a heat-accumulating material with phase transition taking into account the process of solar energy accumulation. Eastern-European Journal of Enterprise Technologies, 6 (8 (120)), 26–37. doi: https://doi.org/10.15587/1729-4061.2022.268618*

1. Introduction

The problems of energy saving and the creation of energy-efficient buildings are relevant for the housing sector of many countries. Residential structures must meet a number of requirements, such as, for example, the shape [1–3], the orientation of the building [4, 5], the materials used to conserve energy [6–8], and the mechanisms

Copyright © 2022, Authors. This is an open access article under the Creative Commons CC BY license

for heating/cooling the premises to create a favorable climate [9–11], etc.

Methods of accumulating heat obtained primarily from renewable energy sources have recently become particularly popular in the field of creating energy-efficient residential buildings. In particular, the use of the heat of solar radiation is described in works [12–14] in the creation of new window structures and facades. The implementation of the heat accumulation function is most often carried out through the use in enclosing structures of substances undergoing phase transitions during a cyclic daily change in the outside air temperature. Among the works in this area, worth noting are [15, 16].

However, despite the popularity of this kind of enclosing structures, they have a number of drawbacks. Thus, when using energy-accumulating enclosing structures with elements of substances with a phase transition, there is a risk of increasing the flammability of the enclosing structure, as well as the ability to release toxic substances during thermal destruction and aging [17]. As another drawback of enclosing structures of this type, one can note their «binding» to a specific region of the building placement, i.e., the need to calculate their parameters taking into account the climatic characteristics of the region. Thus, the task of designing effective enclosing structures that accumulate the energy of solar radiation is still relevant. Its solution will lead to energy savings and costs for the reconstruction and construction of facilities for the storage and transportation of raw materials used to generate energy, for example, industrial pipelines [18], tanks using composite material [19, 20], conventional steel tanks [21, 22], and other shell structures [23–25].

2. Literature review and problem statement

In the modern scientific literature, there is a large body of research on the selection and optimization of energy-accumulating enclosing structures in order to eliminate the above shortcomings. A special place among the well-known scientific research belongs to the development of methods for studying the process of energy accumulation itself. Experimental field studies [13] and methods of classical mathematical modeling [14, 15] are actively used, which in all these cases requires a large amount of costs and time, respectively. Obviously, without mobile mathematical tools, it is impossible to conduct multivariate studies of the developed enclosing structures and choose a rational design in the shortest possible time. Standard verified CFD packages (ANSYS Fluent, PHOENICS, OpenFOAM, etc.) have become widespread for modeling thermophysical processes. These packages are also used in solving problems of construction thermophysics, in particular for the study of thermophysical processes occurring in enclosing structures with heat-accumulating material (HAM) with a phase transition [16]. At the same time, it should be noted that in such CFD packages, the modeling of convective-conductive heat transfer is carried out by the Navier-Stokes equation, averaged by Reynosldsand the thermal conductivity equation. Despite the fact that, as a rule, it is possible to describe the ongoing thermophysical process quite accurately, the main disadvantage of CFD packages is the long calculation time.

The design of external enclosures contributed to the development of passive heat use systems for solar energy, the structure of which combines layers with high heat accumulation capacity and a heat-insulating light-permeable layer [26]. In the process of insolation by sunlight, the light-permeable layer passes the sun's rays to the inner layer. Also, due to the greenhouse effect, this layer prevents the transfer of heat in the opposite direction by radiation, thermal conductivity, and convection from the surface of the heat-accumulating layer. In this case, the inner layer of heat-accumulating material can be made solid or with ventilation channels and a ventilated air gap [27]. In the first case, there is an accumulation of heat in the layer and transfer to the inner surface of the enclosure. In the second case, the heat of solar radiation is used to heat the ventilation air from the room. However, the use of ettringite materials in concrete walls will reduce the mechanical characteristics of the structure and is only suitable for lightweight buildings.

Studies [28, 29] reported extensive comparison of the environmental characteristics of different thermal energy storage materials, including phase-transition materials, thermochemical materials, and sorption materials. However, these studies discuss the methodological basis of the study and present the results of the environmental assessment of the selected materials.

Heat-accumulating materials (HAM) with phase transition with latent heat are very popular due to their high storage density and constant temperature during the phase transition [30]. The main requirement for the application of HAM in buildings and the study of the impact of their use on the indoor environment and the energy efficiency of the building is the correct determination of the thermophysical properties of HAM. Therefore, the design and modeling of HAM cannot be performed without verified input data and their properties [31] but the work reports results of numerical analysis using a biocomposite (biochar) without comparative data with other HAM.

Among the most environmentally friendly organic materials, paraffins are more suitable HAM for residential buildings. Since the melting point of paraffins depends on the number of carbon atoms, these materials have a wide range of applications for accumulating various thermal energy, including solar energy [32]. One of the disadvantages of paraffins is their high flammability. However, due to their non-corrosive properties, paraffins can be encapsulated in a number of metallic and other materials [33], which makes it possible to overcome the risk of HAM leakage and eliminate interaction with the building structure. The use of alternative solar energy in buildings has its own characteristics related to the number of stories of the building, the complexity of the planning solution of objects, and the heat supply scheme [34].

Study [35] describes the energy-saving design of an external enclosure with an energy-active panel. This panel increases the energy activity and heat storage capacity of the external enclosure of the building through the use of a wall panel with heat-accumulating material and inclusive elements [36]. The panel intensifies the heat exchange between the air channel in the enclosure [37], the housing and the heat-accumulating material in the panel. According to the results reported in [38], it is shown that the inclusion of 5 % microencapsulated HAM in concrete can save up to 12 % of thermal energy for heating the room. In addition, the inclusion of HAM in building structures can reduce room temperature fluctuations when external temperatures change. Thus, the content of commercial paraffin of about 30 % in concrete walls can reduce daytime temperatures by 10 °C [39]. In addition to concrete, HAM can be included in frame walls made of light wood, windows, and other structures [40]. It follows that integrating HAM into building components works well to maintain a comfortable temperature inside buildings.

Despite the fact that there are many research methods for developing a qualitative and accurate HAM model discussed in this section, the question of studying the advantages and disadvantages of using HAM remains open. This is due to the fact that for the practical use of HAM it is necessary to accurately determine the parameters and structures of buildings, to study the thermal characteristics of building materials containing HAM, where the timing of the selection and modeling of the appropriate structure is also important.

Taking into account the above, it is justified to conduct a study aimed at building a simplified mathematical model of heat transfer in enclosing structures with HAM.

3. The aim and objectives of the study

The purpose of this study is to construct a simplified mathematical model of heat transfer in enclosing structures with HAM, which could significantly reduce the time of calculations for the development of a high-quality and accurate model of the enclosing structure with HAM.

To accomplish the aim, the following tasks have been set:

– to select and substantiate the structure of the mathematical model of an energy-active enclosing structure with HAM, which has the feature that HAM is contained in a rectangular panel;

– to calculate the process of accumulation of solar energy in the enclosing structures of buildings using inserts with materials with a phase transition.

4. The study materials and methods

The problem was considered in a conjugate statement, taking into account the convective heat exchange between the structural elements and the air moving in the air gaps and the supply system, and the removal of air from the room. Radiant heat exchange was taken into account both with the environment (primarily the effect of insolation) and between the structural elements of the enclosing structure. This is justified since in the processes of heat exchange in the considered variants of enclosing structures, a significant role, in addition to thermal conductivity through solid structural elements, is played by convective and radiant components of heat transfer.

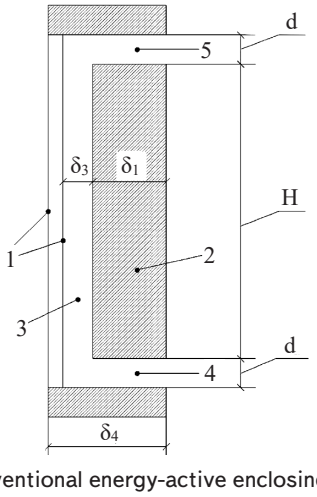

Fig. 1. Conventional energy-active enclosing structure: 1 — double-glazed window; 2 — bearing layer; 3 — air gap; 4 — supply channel; 5 — outlet channel

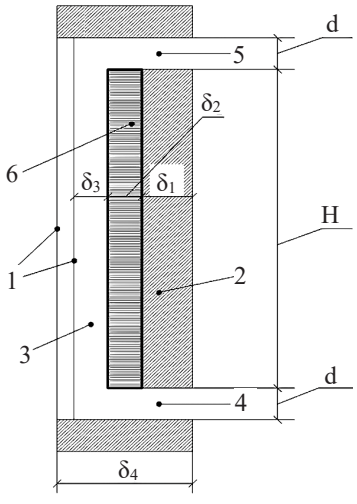

Fig. 2. Energy-active enclosing structure with heat-accumulating material with phase transition: 1 — double-glazed window; 2 — bearing layer; 3 — air gap; 4 — supply channel; 5 — outlet channel; 6 — heat-accumulating material with phase transition

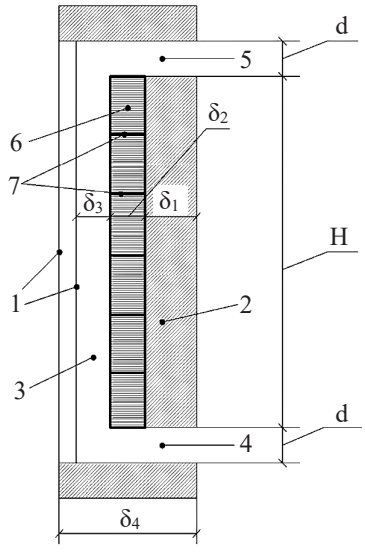

Fig. 3. Energy-active enclosing structure with partitions in the energy-active panel: 1 — double-glazed window; 2 — bearing layer; 3 — air gap; 4 — supply channel; 5 — outlet channel; 6 — heat-accumulating material with phase transition; 7 — metal partitions

When constructing a mathematical model of thermal processes, the options for enclosing structures shown in Fig. 1–3 were considered.

In the above structures (Fig. 1–3), the following assumptions were accepted:

1. The unevenness of the temperature field in the horizontal direction along the enclosing structure (that is, in the direction of the coordinate perpendicular to the sections shown in Fig. 1–3) was neglected due to the fact that the length of the fragment of the enclosing structure in question is quite large.

2. Heat exchange on the upper and lower faces of fragments of enclosing structures depicted in Fig. 1–3 was neglected.

3. The processes of absorption and emission of radiative heat by air masses contained in the layers of the enclosing structure were not considered. At the same time, it was believed that only glasses and an energy-active panel take

part in radiant heat transfer. The participation of other surfaces in radiant heat transfer is insignificant due to their size and orientation.

4. The weakening of insolation due to cloudiness was not taken into account, in other words, sunny days were considered. When simulating several days of operation of an energy-active enclosing structure, a change in the duration of daylight was neglected.

5. It was believed that the spread of thermal disturbances in glasses occurs quite quickly compared to changes in thermal effects external to them (both from the street and from the side of the energy-active panel). In other words, the thermophysical process in the double-glazed window is quasi-stationary. Heat flows in glass in the vertical direction were also neglected, due to its relatively small thickness and insignificant change in temperature vertically.

6. Free-convective motion of the liquid phase of HAM was not considered. If its temperature at some point is in the range between liquidus and solidus, then the motion of the molten components in it will be blocked by the still unmelted components. The movement of HAMFP in the zone of total melt (above the liquidus point) was also neglected due to the fact that it is in a narrow layer [41, 42]. At the same time, we did not consider separately the subregion in which the phase transition occurs and record a detailed mathematical model in the form of a Stephan problem, describing the movement of the phase transition front [41, 42]. The approach [42] was applied, which makes it possible to describe the process of heat transfer by a single equation of thermal conductivity by combining the specific heat of the phase transition and the true heat capacity of HAMFP into the coefficient of effective heat capacity c_{ef}:

$$c_{ef} = \begin{cases} c, & \text{at} \quad T < T_{sol} \quad \text{or} \quad T > T_{liq}, \\ c + \dfrac{L}{T_{liq} - T_{sol}}, & \text{at} \quad T_{sol} < T < T_{liq}, \end{cases} \tag{1}$$

where L is the specific heat of the phase transition; T_{sol} – solidus; T_{liq} – liquidus; $c=c(T)$ is the true specific heat; T is the temperature.

5. Results of the construction of a simplified mathematical model of heat transfer in enclosing structures with heat accumulation material with phase transition

5. 1. Selection and substantiation of the structure of the model of the enclosing structure with a heat-accumulating material with a phase transition on the example of energy-active enclosing structures

A mathematical model of heat exchange in enclosing structures with HAM was built on the example of energy-active enclosing structures, in which HAM is contained in a rectangular panel fixed on the bearing layer of the enclosing structure, as shown in Fig. 1. The outer layer of this structure is made in the form of a double-glazed window made of two glasses 1, through which solar radiation passes. The double-glazed window separates the air gap from the bearing layer 2. To remove the accumulated heat inside the room in the bearing layer, the supply 4 and exhausting 5 air channels are organized. On the surface of the bearing layer, there is an energy-active panel made in the form of a layer of HAM 6, enclosed in a thin metal case. Commercial paraffin with a fairly low melting point is considered as HAM.

Fig. 2 shows a version of the energy-active panel, in which it is divided into chambers by horizontal metal partitions 7, which improve the thermal conductive properties of the panel.

A comparison of the proposed options for the energy-active panel with the conventional one, which does not contain HAM (Fig. 1), was carried out.

The separation of accumulated heat and its transfer to the room is carried out as a result of convective heating of air in gap 3 when it comes into contact with the surface of the bearing energy-active panel (Fig. 2, 3) and the subsequent removal of heated air into the room. Such a flow can be organized in two ways:

– due to natural thrust, in the system the supply channel 4 – air gap 3 – the outlet channel 5, which arises as a result of heating the air in gap 3;

– due to the injection of air by a fan installed in the supply channel 3.

At the same time, in cases where a sufficient amount of heat has not accumulated in the enclosing structure or when there is no need to transfer heat to the room, the movement of air can be blocked by turning off the fan and closing the channels.

As a result of simplifications, the temperature field in the energy-active panel and the bearing layer can be described by a non-stationary two-dimensional heat-conductivity equation:

$$c\rho\frac{\partial T}{\partial t} = \frac{\partial}{\partial x}\left(\lambda\frac{\partial T}{\partial x}\right) + \frac{\partial}{\partial y}\left(\lambda\frac{\partial T}{\partial y}\right), \tag{2}$$

where c is the specific heat capacity (effective (1) for HAM and true for other materials); ρ – density; T – temperature; t – time; x, y – spatial coordinates; λ – thermal conductivity.

It should be noted that even if the change in the thermal conductivity coefficients of materials as a function of temperature can be neglected, equation (2) is nonlinear due to the dependence on the temperature of the effective heat capacity (1).

Equation (2) is considered only in a rectangular spatial region, of width $\delta_1+\delta_{\text{TAM}}$ and height H (Fig. 1, 2). The origin of the Cartesian rectangular coordinate system is in the lower left corner of the energy-active panel. At the boundaries of this calculation area, the following boundary conditions are specified:

To the right:

$$\lambda\frac{\partial T}{\partial x}\bigg|_{x=\delta_1+\delta_{TAM}} = \alpha_{int}\left(T_{int} + T\big|_{x=\delta_1+\delta_{TAM}}\right). \tag{3}$$

At the top:

– during heat extraction (channels are open):

$$\lambda\frac{\partial T}{\partial y}\bigg|_{y=H} = \alpha_{ch\,out}\left(T_{out} - T\big|_{y=H}\right); \tag{4}$$

– when accumulating heat (channels are closed):

$$\lambda\frac{\partial T}{\partial y}\bigg|_{y=H} = 0. \tag{5}$$

At the bottom:

– during heat extraction (channels are open):

$$\lambda\frac{\partial T}{\partial y}\bigg|_{y=0} = \alpha_{ch\,in}\left(T\big|_{y=0} - T_{int}\right); \tag{6}$$

– when accumulating heat (channels are closed):

$$\lambda \left.\frac{\partial T}{\partial y}\right|_{y=0} = 0, \quad (7)$$

where $\alpha_{ch\ in}$, $\alpha_{ch\ out}$ are the heat transfer coefficients on the wall of the supply and discharge channels; T_{int} – indoor air temperature; T_{out} is the air temperature in the outlet channel.

To the left:

$$\lambda \left.\frac{\partial T}{\partial x}\right|_{x=0} = \alpha_{ef}\left(T\big|_{x=0} - T_{ext}\right) - q_{irr}, \quad (8)$$

where α_{ef} is the heat transfer coefficient from the surface of the energy-active panel $x=0$ to the environment; T_{ext} – outdoor temperature; q_{irr} is the density of the heat flux of solar radiation absorbed by the surface of the energy-active panel.

$$q_{irr} = \varepsilon_{HAM} \cdot T_{gl} \cdot T_{gl} \cdot q_{ins}. \quad (9)$$

To calculate the intensity of solar radiation q_{ins} falling on a vertical surface, we use the ASHRAE 2009 model [43] together with the daily change in the position of the Sun in the sky.

A mathematical model of the equations of the quasi-stationary process of heat transfer from the surface of a heat-accumulating structural element (HASE) to the environment was built using dependences describing conductive-convective heat transfer through vertical air gaps and one-dimensional equations of thermal conductivity through a flat wall. For this, the height-average temperatures of the glasses were considered.

Let us introduce the following symbols:

– T_{gl11} – temperature of the outer surface of the outer glass;

– T_{gl12} – temperature of the inner surface of the outer glass;

– T_{gl21} – temperature of the outer surface of the inner glass;

– T_{gl22} – the temperature of the inner surface of the inner glass.

– T_{ac} – averaged height of the surface temperature of the energy-active panel:

$$T_{ac}(t) = \int_0^H T(0,y,t)\,\mathrm{d}y \Big/ H. \quad (10)$$

It should be noted that these temperatures depend only on time.

To describe the conductive-convective heat transfer through vertical air gaps between the flat walls, a model of heat transfer through a fixed layer with an effective coefficient of thermal conductivity λ_k [44] was used, which takes into account both convection and thermal conductivity, and is determined as follows:

$$\lambda_{ef} = \lambda_b \text{ at } \mathrm{Ra} < 10^4,$$

$$\lambda_{ef} = \lambda_b \cdot 0.062 \cdot \mathrm{Ra}^{1/3} \text{ at } 10^4 < \mathrm{Ra} < 10^7, \quad (11)$$

$$\lambda_{ef} = \lambda_b \cdot 0.22 \cdot \mathrm{Ra}^{1/4} \text{ at } 10^7 < \mathrm{Ra} < 10^{10},$$

where λ_b is the true value of the coefficient of thermal conductivity of air; $\mathrm{Ra} = \dfrac{g\delta^3\beta\Delta T}{\nu}\mathrm{Pr}$ is the Rayleigh number; g is the acceleration of free fall; δ – thickness of the air gap; β – the coefficient of volumetric thermal expansion, which for air in the case of normal conditions can be taken to be equal to 1/273 K; ΔT is the temperature difference on the opposite walls of the air gap; ν – coefficient of kinematic viscosity of air; Pr is the Prandtl number.

The values λ_b, ν and Pr and Pr when using expressions (11) are taken at average values of temperature and pressure in the air gap. Obviously, the pressure drop in this case can be neglected and taken to be equal to one atmosphere.

For the air gap inside the double-glazed window, the Rayleigh number is of the form:

$$\mathrm{Ra}_{gl}(t) = \frac{g\delta_{bgl}^3\beta\left(T_{gl21}(t) - T_{gl12}(t)\right)\Delta T}{\nu}\mathrm{Pr}, \quad (12)$$

and for the air gap between the double-glazed window and the energy-active panel:

$$\mathrm{Ra}_b(t) = \frac{g\delta_b^3\beta\left(T_{gl22}(t) - T_{ac}(t)\right)\Delta T}{\nu}\mathrm{Pr}. \quad (13)$$

In this case, in the first air gap, the values of λ_b, ν and Pr are taken at a temperature $(T_{gl21}(t)+T_{gl12}(t))/2$, and in the second air gap at a temperature $(T_{gl22}(t)+T_{ac}(t))/2$.

As a result, using a one-dimensional mathematical model of heat transfer through a flat plate, the following ratios can be recorded for the density of heat flux passing through air gaps and glasses.

$$q(t) = \lambda_{gl} \cdot (T_{gl12}(t) - T_{gl11}(t))/\delta_{gl} + q_{r1}, \quad (14)$$

$$q(t) = \lambda_{ef\,gl}(t) \cdot (T_{gl21}(t) - T_{gl12}(t))/\delta_{b\,gl} + q_{r2}, \quad (15)$$

$$q(t) = \lambda_{gl} \cdot (T_{gl22}(t) - T_{gl21}(t))/\delta_{gl} + q_{r3}, \quad (16)$$

$$q(t) = \lambda_{ef\,b}(t) \cdot (T_{ac}(t) - T_{gl22}(t))/\delta_b + q_{r4}, \quad (17)$$

where λ_{gl} is the thermal conductivity of the glass; δ_{gl} – glass thickness; $\delta_{b\,gl}$ – the thickness of the air gap in the double-glazed window; δ_b – the thickness of the air gap between the double-glazed window and the energy-active panel; q_r is the radiant component of the heat flux, which is derived from the Stefan-Boltzmann equation.

The heat flow from the surface of the outer glass to the environment is as follows:

$$q(t) = \alpha_{ext} \cdot (T_{gl11} - T_{ext}), \quad (18)$$

where α_{ext} is the heat transfer coefficient, which takes into account not only the convective, but also the radiant component of heat exchange with the environment.

Due to the assumption of the quasi-stationarity of the heat transfer process through the air gap and the double-glazed window, the left-hand parts of equations (14) to (18) are equal to each other.

It should be noted that equations (15), (17) are nonlinear algebraic equations since the effective coefficients of thermal conductivity $\lambda_{ef\,gl}$ and $\lambda_{ef\,b}$ nonlinearly depend on the corresponding Rayleigh numbers, which in turn are nonlinearly dependent on the temperatures $T_{ac}(t)$, $T_{gl22}(t)$, $T_{gl21}(t)$ and $T_{gl12}(t)$.

As a result, the expression for the coefficient of heat transfer α_{ef} in expression (8) can be written using the ratios for thermal resistance of the multilayer structure, as follows:

$$\alpha_{ef}(t) = \left(\frac{1}{\alpha_{ext}} + \frac{\lambda_{gl}}{\delta_{gl}} + \frac{\lambda_{ef\,gl}(t)}{\delta_{b\,gl}} + \frac{\lambda_{gl}}{\delta_{gl}} + \frac{\lambda_{ef\,b}(t)}{\delta_b}\right)^{-1}. \quad (19)$$

To find the air temperature in the outlet channel T_{out}, write down the expression for the amount of heat per unit time Q spent on heating the air when it passes in the air gap between the double-glazed window and the energy-active panel:

$$Q(t)=c_p(t)\cdot G(t)\cdot(T_{out}(t)-T_{int}(t)), \quad (20)$$

where c_p is the heat capacity of the air at averaged values of temperature and pressure in the air gap; G is the mass flow rate of air.

On the other hand, this same amount of heat can be produced as the difference between the amount of heat supplied to the air through the surface of the energy-active panel and the amount of heat drawn from the air through the double-glazed window:

$$Q(t)=F\cdot\alpha_b(t)\cdot(T_{ac}(t)-T_b(t))-F\cdot\alpha_b(t)\cdot(T_b(t)-T_{gl22}(t)), \quad (21)$$

where F is the surface area of the energy-active panel, it is also the area of the double-glazed window; α_b – the heat transfer coefficient, which we take to be the same on the surface of HASE and on the glass; T_c is the average value of the air temperature in the gap.

Equating the right parts (20) and (21) and assuming $T_b(t)=(T_{out}(t)+T_{int}(t))/2$, the following is obtained:

$$c_p(t)\cdot G(t)\cdot(T_{out}(t)-T_{int}(t))=$$

$$=F\cdot\alpha_b(t)\cdot(T_{ac}(t)+T_{gl22}(t)-T_{out}(t)-T_{int}(t)). \quad (22)$$

Considering:

$$F=B\cdot H,$$

$$G=\rho_b\cdot B\cdot\delta_b\cdot v,$$

where B is the length of the considered energy-active enclosing structure in the horizontal direction, ρ_b is the density of air averaged over the gap, v is the velocity of the air flow in the gap, expression (22) produces the following equation for finding $T_{out}(t)$:

$$c_p(t)\cdot\rho_b(t)\cdot\delta_b\cdot v(t)\cdot(T_{out}(t)-T_{int}(t))=$$

$$=H\cdot\alpha_b(t)\cdot(T_{ac}(t)+T_{gl22}(t)-T_{out}(t)-T_{int}(t)). \quad (23)$$

Speed $v(t)$ can be determined from the volumetric flow rate of air through the gap, which, in turn, is calculated from the pressure difference. Pressure is generated by the fan and atmospheric pressure (in the case of air injection into the gap by a fan) or from the pressure difference due to the expansion of the air when heated (in the case of natural thrust in the air gap). Heat capacity $c_p(t)$ and density $\rho_b(t)$ are taken at atmospheric pressure and the average temperature and pressure in the air gap $T_b(t)=(T_{out}(t)+T_{int}(t))/2$.

The coefficient of heat transfer α_b on the surface of the glass unit and HASE, as well as the coefficients of heat transfer $\alpha_{ch\,in}$, $\alpha_{ch\,out}$ on the surfaces, are calculated on the basis of the relationships between the Nussleit and Reynolds numbers for forced convection in the channels [41].

Having solved equation (23) with respect to $T_{out}(t)$, it is possible to obtain the value of the air temperature in the exhaust channel. Note that since the properties of air c_p and ρ_b and the heat transfer coefficient α_b depend on the averaged air temperature, which, in turn, is calculated on the basis of the value of T_{out}, then (23) is a nonlinear algebraic equation.

The initial conditions for equation (2) were determined on the basis of the solution of the stationary analog of the above mathematical model. It was also believed that $q_{ins}=0$. From a physical point of view, this would almost correspond to the fact that at the initial moment of time the thermal state of the enclosing structure was set, established before dawn after several days, where external weather conditions remained unchanged, and daytime solar radiation was significantly weakened by a dense layer of clouds. It is possible to assign another set of initial conditions that can be obtained as a result of solving an auxiliary non-stationary problem that simulates the operation of the enclosing structure in question for several days under conditions of periodic external influences. This process proceeded until the steady-state temperature regime was reached, which does not depend on the initial conditions of this auxiliary non-stationary problem.

Since the above mathematical model is nonlinear and contains both a partial differential equation with initial and boundary conditions and algebraic equations, an iterative process was used to solve it.

The non-stationary equation of thermal conductivity (2) was solved by the method of finite differences, for which a finite difference approximation of equation (2) and boundary conditions (3) to (7) was written. During the transition in the decision process from the k-1 time layer of the difference grid to the k-th time layer, the following procedure was used to calculate the values of the heat transfer coefficient α_{ef} and the temperature T_{out}. Since they appear in the resulting difference scheme.

Based on the temperature values obtained on the $k-1$ time layer, the surface temperature of the energy-active panel $T_{ac}^{(k-1)}$ was calculated according to the numerical integration of expression (10) in the nodes of the difference stack. Assuming $T_{ac}(t)=T_{ac}^{(k-1)}$ in equation (17), we obtained a system of five algebraic equations (14) to (18) with five unknowns $T_{gl11}(t)$, $T_{gl12}(t)$, $T_{gl21}(t)$, $T_{gl22}(t)$, $q(t)$, each of which corresponds to a time point t_k. This nonlinear system is solved by simple iterations by moving from the surface of the energy-active panel to the outer surface of the glass unit. As an initial approximation for the values T_{gl11}, T_{gl12}, T_{gl21}, T_{gl22}, in such an iterative process, the values of the desired temperatures found in the previous time step are taken: T_{gl11} (t_{k-1}), T_{gl12} (t_{k-1}), $T_{gl21}(t_{k-1})$, $T_{gl22}(t_{k-1})$. As a result of this iterative solution of the system of equations (14) to (18), we find both temperature values $T_{gl11}(t_k)$, $T_{gl12}(t_k)$, $T_{gl21}(t_k)$, $T_{gl22}(t_k)$ and the values of the effective coefficients of thermal conductivity $\lambda_{ef\,gl}$, $\lambda_{ef\,b}$ on the k-th time step. Then, using these values, the heat transfer coefficient $a_{ef}^{(k)}$ was found according to (19).

If, at the k-th time, the accumulated heat is selected, then it is also necessary to solve equation (23) assuming $T_{ac}(t)=T_{ac}(t_{k-1})$ and $T_{gl22}(t)=T_{gl22}(t_k)$. As a result of its solution, we obtain the current value of $T_{out}(t_k)$, and simultaneously find the current value of the mass flow rate G, on the basis of which it will be possible to calculate the values of the heat transfer coefficients $\alpha_{ch\,in}(t_k)$ and $\alpha_{ch\,out}(t_k)$.

Knowing $\alpha_{ef}(t_k)$ (as well as $\alpha_{ch\,in}(t_k)$ and $\alpha_{ch\,out}(t_k)$ in the case of heat extraction at the k-th point in time), it is possible to solve the equations of the difference scheme that approximate the thermal conductivity equation and boundary conditions, and to find the temperature values in the nodes of the difference grid for the k-th point in time.

At the end of all these calculations, in the k-th time step, it is possible, multiplying by a time step the value found

according to (20), to obtain the amount of usable heat selected from the energy-active enclosing structure in the interval between the $k-1$ and k-th moments of time.

5. 2. Calculation of the process of accumulation of solar energy in the enclosing structures of buildings using a phase transition

The given mathematical model and the procedure for modeling thermal processes in energy-active enclosing structures were used for a comparative analysis of the above-described options for the execution of the enclosing structure.

Results for five versions of energy-active enclosing structures. Option 1 corresponds to Fig. 1 with the design parameters given in Table 1. Option 2 corresponds to Fig. 2 with the design parameters given in Table 1. Option 3 corresponds to Fig. 3 with the design parameters given in Table 1 for the case of high-thermally conductive inclusions that break a heat-accumulating material with a phase transition in an energy active panel into five chambers. Option 4 differs from Option 3 in doubling the number of high-thermal inclusions. Option 5 corresponds to Fig. 2 with the design parameters given in Table 1, with the application of a heat-reflecting coating of aluminum foil to the surface of the energy-active panel.

For a comparative analysis of energy-active enclosing structures, their operation for two days under the most extreme conditions was considered, namely at the shortest daylight hours and under the conditions of the coldest five-day week in Shymkent (Republic of Kazakhstan). According to the normative documents of the Republic of Kazakhstan in the sector of architecture and construction, the following values were adopted: $T_{ext}=-15$ °C; $T_{int}=20$ °C; $\alpha_{ext}=23$ W/(m^2·K); $\alpha_{int}=8.7$ W/(m^2·K). The length of daylight was taken to be 9 hours, which roughly corresponds to this parameter during the winter solstice at the latitude of Shymkent.

As a determining parameter when comparing energy-active enclosing structures, the amount of energy E_A, which is accumulated in the enclosing structure, with an area of 1 m^2, was considered.

The selection of accumulated heat began immediately after sunset. It continued until the surface temperature of the heat-accumulating structural element, as a result of the selection of heat accumulated during daylight hours, did not drop to a value corresponding to the air temperature in the room, Tables 2, 3.

Table 1

Parameters of energy-active enclosing structures

Parameter	Variant 1	Variant 2	Variant 3
Bearing layer thickness, δ_1, mm	400	300	300
Thickness of energy-active panel, δ_{HAM}, mm	–	100	100
Air clearance width, δ_b, mm	120	120	120
Thickness of window glass δ_{gl}, mm	4	4	4
Distance between glasses, $\delta_{b\,gl}$, mm	12	12	12
Thickness of partitions in TAMFP, mm	–	–	2
Number of partitions in TAMFP	–	–	4
Height of energy-active panel H, mm	1400	1400	1400
Material of the bearing layer	bricklay	bricklay	bricklay
Material of the body of the energy-active panel and partitions	–	steel	steel
Thermal conductivity TAMFP, W/(mK) [45]	0.21	0.21	0.21
Heat capacity of TAMFP, kJ/(kgK) [45]	2.1	2.1	2.1
TAMFP density, kg/m^3	900	900	900
Melting point TAMFP, C°	28–41	28–41	28–41
Specific heat of TAMFP melting, kJ/kg	200	200	200

Table 2

Mode parameters of energy-active enclosing structures in the first day of solar energy accumulation in the case of selection of accumulated heat due to natural thrust

Parameter, units of measurement	Variant 1	Variant 2	Variant 3	Variant 4	Variant 5
Temperature of the outer surface of HASE at sunrise, °C	–4.0	–5.3	–4.3	–3.7	–5.3
Maximum temperature of the outer surface of HASE, °C	85.7	67.6	59.8	52.9	20.1
Time to reach the maximum surface temperature of HASE, hour:minute	5:57	5:47	5:52	5:58	6:06
Temperature of the outer surface of HASE at the time of the beginning of the extraction of usable heat, °C	48.0	39.2	38	36.9	9.9
Maximum temperature at the point of contact of HASE with the bearing layer, °C	40.9	21.5	23.0	25.6	9.3
Time to reach the maximum temperature at the point of contact of HASE with the load layer, h:m	8:55	18:01	15:17	13:16	12:32
Maximum accumulated heat, MJ (1 m^2)	14.5	16.7	17.5	18.3	3.9
Time to reach the maximum accumulated heat, h:m	8:13	8:32	8:33	8:35	8:19
Accumulated heat at the time of the beginning of the selection of usable heat, MJ	14.1	16.5	17.3	18.2	3.8
Selected usable heat per day	0.91	1.78	1.79	1.79	–
Duration of usable heat extraction, h:m	3:12	6:54	7:08	7:17	–
Heat loss from sunset to sunrise, MJ	6.3	6.2	6.6	6.8	1.5

Table 3

Mode parameters of energy-active enclosing structures on the second day of solar energy accumulation in the case of selection of accumulated heat due to natural thrust

Parameter, units of measurement	Variant 1	Variant 2	Variant 3	Variant 4	Variant 5
Surface temperature of HASE at sunrise, °C	6.3	7.2	10.6	12.2	–2.2
Maximum surface temperature of HASE, °C	91.5	73.3	65	57.7	22.2
Time to reach the maximum surface temperature of HASE, h:m	29:52	30:01	30:01	30:04	30:03
Surface temperature of HASE at the time of the beginning of the extraction of usable heat, °C	52.9	40.0	39.2	38.5	11.8
Maximum temperature at the point of contact of HASE with the bearing layer, °C	49.3	26.5	27.8	29.1	11.9
Time to reach the maximum temperature at the point of contact of HASE with the bearing layer, h:m	32:47	46:41	41:39	38:36	35:50
Maximum accumulated heat, MJ	19.3	23.6	24.6	25.9	5.7
Time to reach the maximum accumulated heat, h:m	32:01	32:23	32:25	32:27	32:07
Accumulated heat at the time of the beginning of the selection of usable heat, MJ	18.8	23.4	24.4	25.7	5.6
Selected usable heat per day	1.4	2.2	2.5	2.8	–
Duration of usable heat extraction, hour:minute	4:36	9:03	10:38	12:01	–
Heat loss from sunset to sunrise, MJ	8.4	8.2	8.6	9.0	2.2

Fig. 4–7 show the above options for energy-active enclosing structures during the first 48 hours after the change of cloudy weather to clear. The beginning of the countdown corresponds to the sunrise on the first clear day. After each sunset, the accumulated thermal energy is selected due to forced convection as a result of pressure injection by a fan in the supply channel. The numbering of the curves corresponds to the serial numbers described above of the three schemes of the enclosing structure. Fig. 4 shows the change in altitude-averaged temperature on the surface absorbing solar radiation.

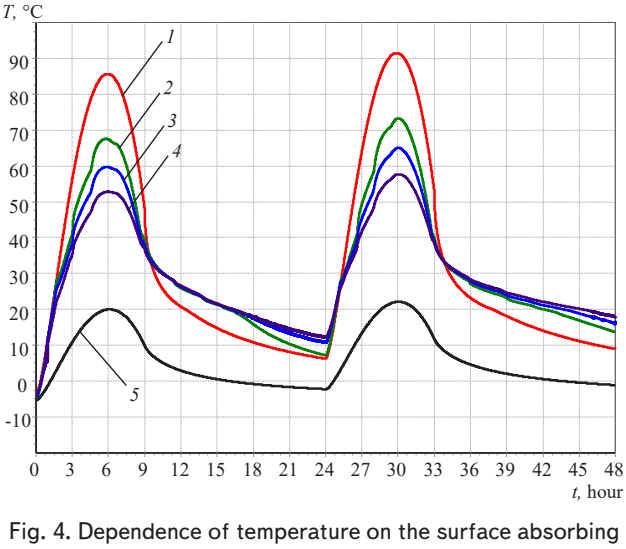

Fig. 4. Dependence of temperature on the surface absorbing solar radiation on time: 1 — option 1; 2 — option 2; 3 — option 3; 4 — option 4; 5 — option 5

Fig. 5 shows the amount of thermal energy accumulated in the enclosing structure, starting from the zero moment of time, per 1 m^2. Fig. 6 – a temperature change at the junction of the energy-active panel and the bearing layer of the enclosing structure averaged in height (for option 1 – the change in temperature in the bearing layer of the depth corresponding to the thickness of the energy-active panel considered in other variants). Fig. 7 shows the amount of usable thermal energy selected from the accumulating element and allocated to the room, based on 1 m^2 of the enclosing structure.

As can be seen from the above Fig. 3–6 and Tables 1–3, in the case of HAM, the accumulating element of the enclosing structure heats up faster compared to other versions. The rate of cooling of this surface after the cessation of exposure to solar radiation is also the greatest. Applying a reflective coating to the surface of the energy-active panel significantly reduces the accumulation of heat in it, which is why Option 5 is not shown in Fig. 7.

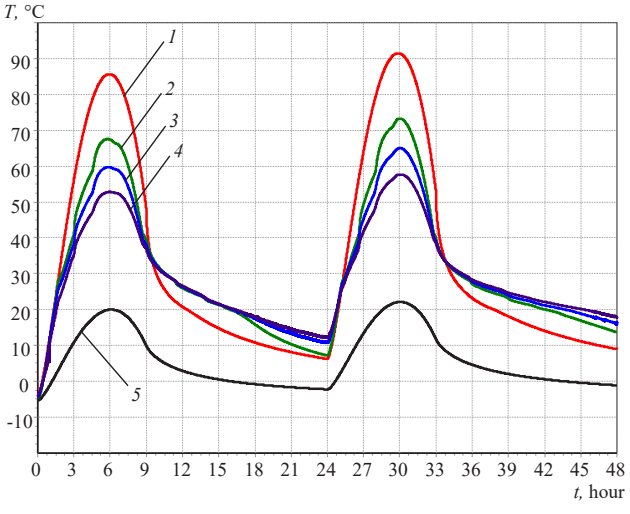

Fig. 5. Accumulation of thermal energy dependent on time indicator: 1 — option 1; 2 — option 2; 3 — option 3; 4 — option 4; 5 — option 5

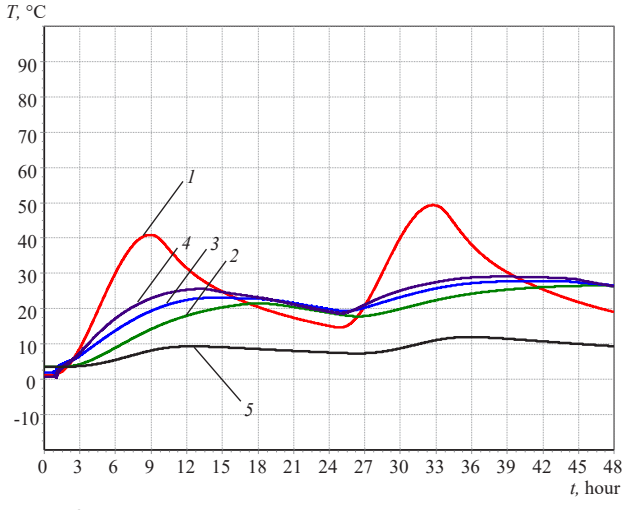

Fig. 6. Dependence of temperature at the junction of the energy-active panel and the bearing layer of the enclosing structure on time: 1 — option 1; 2 — option 2; 3 — option 3; 4 — option 4; 5 — option 5

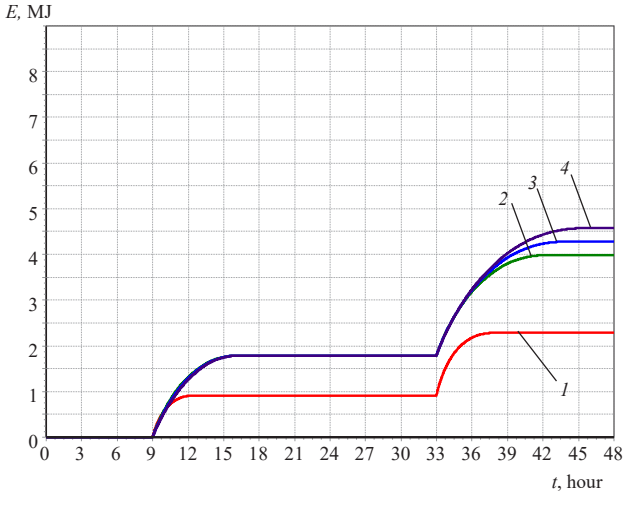

Fig. 7. Usable thermal energy dependent on time indicator: 1 — option 1; 2 — option 2; 3 — option 3; 4 — option 4

6. Discussion of results of investigating the process of accumulation of solar energy in the enclosing structures of buildings using phase transition

Daily temperature maxima on the surface receiving solar radiation are observed at times around 6 and 30 hours, which corresponds to 6 hours after sunrise. Despite the fact that after these moments the enclosing structure is exposed to solar radiation for another 3 hours, the surface temperature begins to decrease due to the fact that the Sun has passed the zenith and the intensity of insolation begins to weaken. The maximum temperature in the second 24 hours exceeds the temperature maximum in the first day by 4–6 °C, depending on the version of the enclosing structure for Options 1–4 and 2 °C for Option 5. The shift of the maximum in time to an earlier moment in the second 24 hours occurs, obviously, because due to the higher temperature on the surface of HASE, heat loss through the double-glazed window increases.

At a depth corresponding to the thickness of the energy-active panel (Fig. 6), the daily temperature maxima are shifted in time to later moments, which differ depending on the design of the enclosing structure. Obviously, this delay in temperature maxima at this point of the enclosing structure compared to the maximums of temperature on the surface is associated with the thermal inertia of HASE, and the difference in the magnitude of this shift in different versions of the enclosing structure is explained by the different ratio between the heat capacity and thermal conductivity of its elements. At the same time, a general pattern is observed: the earliest moments of maxima are characteristic of the variant of the execution of the enclosing structure without HAM with a phase transition (option 1), in the case of the presence of HAM, temperature maxima are observed later, the less high-thermal inclusions are located in HAM. At the same time, it should be noted that at this depth, the temperature, even at the moments of peak heating, does not reach the liquidus point, that is, HAM of the selected thickness does not melt completely at the farthest points from the surface of the energy-active panel that absorbs solar radiation. To choose the optimal thickness of the energy-active panel, which may depend on many factors, both external weather and internal structural, it is necessary to conduct additional research.

As for the amount of heat accumulated in the energy-active enclosing structure, its maximum is reached in 0.5–1.5 hours (depending on the version of the enclosing structure) before sunset (Fig. 5). After this point, the absorbed solar radiation can no longer compensate for heat loss from the surface of HASE through the double-glazed window into the surrounding space, and the amount of accumulated energy begins to decrease. At time points 9 and 33 hours, there is a violation of the smoothness of the curves on the graph, which is caused by a sharp increase in heat dissipation from HASE due to the fact that the extraction of usable heat to heat the room is added to the heat loss to the environment. Fig. 5 shows that the presence of HAM in the enclosing structure (options 2–4) significantly increases the amount of accumulated thermal energy, compared with the accumulation of heat exclusive in the load layer (option 1). At the same time, an increase in the number of high-thermally conductive inclusions contributes to an increase in the heat-accumulating properties of the enclosing structure. At the same time, the application of a reflective coating to the surface of the energy-active panel (option 5) significantly reduces the accumulation of heat in it.

The plots illustrating the change in the amount of usable heat discharged to the room (Fig. 7) demonstrate that the selection of usable heat, which began with the sunset, does not continue throughout the dark part of the day. It lasts only about 5.5 hours on the first day (without HAM – about 2.5 hours) and up to 8 hours (depending on the version of the enclosing structure) on the second day. After that, the temperature of the surface from which the heat is collected drops below the air temperature in the room (Fig. 4), which makes it impossible to collect usable heat. There is also a drop in surface temperature and a decrease in the amount of heat accumulated in the enclosing structure due to heat loss to the environment through the double-glazed window. However, when the moment of sunrise is reached on the second day, there is still residual accumulated heat in the enclosing structure and the temperature of the receiving surface does not have time to drop to the temperature set in the initial conditions. As a result of retaining such residual heat during the subsequent accumulation of solar energy after sunrise in the second 24 hours, the enclosing structure heats up more. Compared to the first day and at the beginning of the selection,

it contains more accumulated heat (Fig. 4, 5). In addition, an increase in the surface temperature of the accumulating element makes it possible to select more usable heat from it on the second day compared to the first.

It should also be noted that the convective movement of HAM melt was not taken into account in the models used. Obviously, the introduction of such motion in the mathematical model in comparison with the results obtained will lead to additional heat transfer from the surface heated by the Sun deep into HASE. As a result, the rate of accumulation of thermal energy and its return during the selection of the usable part in a real situation will be higher. Thus, the accepted assumption about the immobility of HAM melt is conservative, and the calculation of the accumulated energy is performed with a margin.

It should also be noted that a feature of these structures is that a significant part of the accumulated solar energy, which was not used to heat the room, is irretrievably lost during the dark part of the day as a result of heat loss through the double-glazed window. The way out of this situation may be the arrangement of additional air channels inside the energy-active panel, which makes it possible to take heat not only from its surface. Another way to solve this problem may be the intensive removal of the heat accumulated in the enclosing structure into the heat accumulators located inside the building in the first hours after sunset.

It should be noted that the study did not take into account the geometric dimensions of panels with heat-accumulating material, the geometry and number of air channels, the number of partitions, etc. However, these assumptions do not affect the results obtained and can be taken into account in additional tests. The developed structures can be used not only for new designed buildings but also for the reconstruction and thermal modernization of existing facilities.

7. Conclusions

1. The proposed design of the structure, a characteristic feature of which is an energy-active panel containing a heat-accumulating material with a phase transition, makes it possible to accumulate solar radiation during daylight hours, followed by the use of stored energy for heating the room. The structure of the mathematical model of heat transfer includes a non-stationary two-dimensional equation of non-stationary thermal conductivity to determine the temperature state of the bearing layer and the heat accumulating material, as well as algebraic equations describing the quasi-stationary transfer process in the remaining elements of the enclosing structure.

This model and the calculation procedure have a significant advantage in terms of performance. Therefore, the proposed approach to determining the thermal regimes of enclosing structures, based on the use of such a model structure, can be applied in multivariate calculations to optimize their design in order to increase energy efficiency. The most effective options can then be refined using a more accurate model and its computer implementation in a certified CFD package. A similar approach can be used by engineers, designers in the field, as well as when teaching at the university as a mobile method.

2. The proposed calculation procedure was tested when modeling the thermal regimes of several variants of energy-active enclosing structures. The use of heat-accumulating material with a phase transition makes it possible to reduce the temperature of the surface receiving solar radiation during daylight hours compared to the option of heat accumulation only in the bearing layer of the enclosing structure. As a result, the amount of accumulated energy during daylight hours increases significantly (by 15–35 %). At night, the surface temperature of the heat-accumulating element in structures using a material with a phase transition is greater than in the case of heat accumulation only in the bearing layer. As a result, it is possible to select 70–120 % more usable heat. The presence of high-thermal partitions (option 4) in a heat-accumulating material with a phase transition contributes to an increase in accumulated heat and usable heat relative to other options.

Conflicts of interest

The authors declare that they have no conflict of interest in relation to this research, whether financial, personal, authorship or otherwise, that could affect the research and its results presented in this paper.

Financing

The study was conducted without financial support.

Data availability

All data are available in the main text of the manuscript.

References

1. Pacheco, R., Ordóñez, J., Martínez, G. (2012). Energy efficient design of building: A review. Renewable and Sustainable Energy Reviews, 16 (6), 3559–3573. doi: https://doi.org/10.1016/j.rser.2012.03.045
2. Zhangabay, N., Abshenov, K., Bakhbergen, S., Zhakash, A., Moldagaliyev, A. (2022). Evaluating the Effectiveness of Energy-Saving Retrofit Strategies for Residential Buildings. International Review of Civil Engineering (IRECE), 13 (2), 118. doi: https://doi.org/10.15866/irece.v13i2.20933
3. Du, K., Calautit, J., Wang, Z., Wu, Y., Liu, H. (2018). A review of the applications of phase change materials in cooling, heating and power generation in different temperature ranges. Applied Energy, 220, 242–273. doi: https://doi.org/10.1016/j.apenergy.2018.03.005
4. Shi, X., Tian, Z., Chen, W., Si, B., Jin, X. (2016). A review on building energy efficient design optimization rom the perspective of architects. Renewable and Sustainable Energy Reviews, 65, 872–884. doi: https://doi.org/10.1016/j.rser.2016.07.050
5. Martín, M., Villalba, A., Inés Fernández, A., Barreneche, C. (2019). Development of new nano-enhanced phase change materials (NEPCM) to improve energy efficiency in buildings: Lab-scale characterization. Energy and Buildings, 192, 75–83. doi: https://doi.org/10.1016/j.enbuild.2019.03.029

6. Kudabayev, R., Suleimenov, U., Ristavletov, R., Kasimov, I., Kambarov, M., Zhangabay, N., Abshenov, K. (2022). Modeling the Thermal Regime of a Room in a Building with a Thermal Energy Storage Envelope. Mathematical Modelling of Engineering Problems, 9 (2), 351–358. doi: https://doi.org/10.18280/mmep.090208
7. Ren, M., Wen, X., Gao, X., Liu, Y. (2021). Thermal and mechanical properties of ultra-high performance concrete incorporated with microencapsulated phase change material. Construction and Building Materials, 273, 121714. doi: https://doi.org/10.1016/j.conbuildmat.2020.121714
8. Elias, C. N., Stathopoulos, V. N. (2019). A comprehensive review of recent advances in materials aspects of phase change materials in thermal energy storage. Energy Procedia, 161, 385–394. doi: https://doi.org/10.1016/j.egypro.2019.02.101
9. Geetha, N. B., Velraj, R. (2012). Passive cooling methods for energy efficient buildings with and without thermal energy storage – A review. Energy Education Science and Technology Part A: Energy Science and Research, 29 (2), 913–946.
10. Buonomo, B., Capasso, L., Diana, A., Manca, O., Nardini, S. (2019). A numerical analysis on a solar chimney with an integrated latent heat thermal energy storage. AIP Conference Proceedings. doi: https://doi.org/10.1063/1.5138762
11. Feng, P. H., Zhao, B. C., Wang, R. Z. (2020). Thermophysical heat storage for cooling, heating, and power generation: A review. Applied Thermal Engineering, 166, 114728. doi: https://doi.org/10.1016/j.applthermaleng.2019.114728
12. Cuce, E., Cuce, P. M. (2016). Solar Pond Window Technology for Energy-Efficient Retrofitting of Buildings: An Experimental and Numerical Investigation. Arabian Journal for Science and Engineering, 42 (5), 1909–1916. doi: https://doi.org/10.1007/s13369-016-2375-0
13. Irshad, K., Habib, K., Saidur, R., Kareem, M. W., Saha, B. B. (2019). Study of thermoelectric and photovoltaic facade system for energy efficient building development: A review. Journal of Cleaner Production, 209, 1376–1395. doi: https://doi.org/10.1016/j.jclepro.2018.09.245
14. Shen, J., Zhang, X., Yang, T., Tang, L., Shinohara, H., Wu, Y. et al. (2016). Experimental Study of a Compact Unglazed Solar Thermal Facade (STF) for Energy-efficient Buildings. Energy Procedia, 104, 3–8. doi: https://doi.org/10.1016/j.egypro.2016.12.002
15. Zhu, L., Yang, Y., Chen, S., Sun, Y. (2018). Numerical study on the thermal performance of lightweight temporary building integrated with phase change materials. Applied Thermal Engineering, 138, 35–47. doi: https://doi.org/10.1016/j.applthermaleng.2018.03.103
16. Borodulin, V. Y., Nizovtsev, M. I. (2018). Heat-inertial properties of walls of lightweight thermal insulation with phase change materials. Journal of Physics: Conference Series, 1105, 012108. doi: https://doi.org/10.1088/1742-6596/1105/1/012108
17. Vede, P., Kiselkin, E. (2018). Thermal Energy Storage in the Envelope of Buildings. Epoha nauki, 14, 165–173. Available at: http://eraofscience.com/EofS/Vypyski2018/14-iyun_2018/40.pdf
18. Suleimenov, U., Zhangabay, N., Utelbayeva, A., Ibrahim, M. N. M., Moldagaliyev, A., Abshenov, K. et al. (2021). Determining the features of oscillations in prestressed pipelines. Eastern-European Journal of Enterprise Technologies, 6 (7 (114)), 85–92. doi: https://doi.org/10.15587/1729-4061.2021.246751
19. Tursunkululy, T., Zhangabay, N., Avramov, K., Chernobryvko, M., Suleimenov, U., Utelbayeva, A. et al. (2022). Strength analysis of prestressed vertical cylindrical steel oil tanks under operational and dynamic loads. Eastern-European Journal of Enterprise Technologies, 2 (7 (116)), 14–21. doi: https://doi.org/10.15587/1729-4061.2022.254218
20. Suleimenov, U., Zhangabay, N., Utelbayeva, A., Azmi Murad, M. A., Dosmakanbetova, A., Abshenov, K. et al. (2022). Estimation of the strength of vertical cylindrical liquid storage tanks with dents in the wall. Eastern-European Journal of Enterprise Technologies, 1 (7 (115)), 6–20. doi: https://doi.org/10.15587/1729-4061.2022.252599
21. Suleimenov, U., Zhangabay, N., Abshenov, K., Utelbayeva, A., Imanaliyev, K., Mussayeva, S. et al. (2022). Estimating the stressed-strained state of the vertical mounting joint of the cylindrical tank wall taking into consideration imperfections. Eastern-European Journal of Enterprise Technologies, 3 (7 (117)), 14–21. doi: https://doi.org/10.15587/1729-4061.2022.258118
22. Zhangabay, N., Sapargaliyeva, B., Utelbayeva, A., Kolesnikov, A., Aldiyarov, Z., Dossybekov, S. et al. (2022). Experimental Analysis of the Stress State of a Prestressed Cylindrical Shell with Various Structural Parameters. Materials, 15 (14), 4996. doi: https://doi.org/10.3390/ma15144996
23. Zhangabay, N., Sapargaliyeva, B., Suleimenov, U., Abshenov, K., Utelbayeva, A., Kolesnikov, A. et al. (2022). Analysis of Stress-Strain State for a Cylindrical Tank Wall Defected Zone. Materials, 15 (16), 5732. doi: https://doi.org/10.3390/ma15165732
24. Zhangabay, N., Suleimenov, U., Utelbayeva, A., Kolesnikov, A., Baibolov, K., Imanaliyev, K. et al. (2022). Analysis of a Stress-Strain State of a Cylindrical Tank Wall Vertical Field Joint Zone. Buildings, 12 (9), 1445. doi: https://doi.org/10.3390/buildings12091445
25. Tursunkululy, T., Zhangabay, N., Avramov, K., Chernobryvko, M., Suleimenov, U., Utelbayeva, A. (2022). Influence of the parameters of the pre-stressed winding on the oscillations of vertical cylindrical steel oil tanks. Eastern-European Journal of Enterprise Technologies, 5 (7 (119)), 6–13. doi: https://doi.org/10.15587/1729-4061.2022.265107
26. Pintaldi, S., Sethuvenkatraman, S., White, S., Rosengarten, G. (2017). Energetic evaluation of thermal energy storage options for high efficiency solar cooling systems. Applied Energy, 188, 160–177. doi: https://doi.org/10.1016/j.apenergy.2016.11.123
27. Ndiaye, K., Ginestet, S., Cyr, M. (2018). Thermal energy storage based on cementitious materials: A review. AIMS Energy, 6 (1), 97–120. doi: https://doi.org/10.3934/energy.2018.1.97
28. Horn, R., Burr, M., Fr hlich, D., Gschwander, S., Held, M., Lindner, J. P., Munz, G. et al. (2018). Life Cycle Assessment of Innovative Materials for Thermal Energy Storage in Buildings. Procedia CIRP, 69, 206–211. doi: https://doi.org/10.1016/j.procir.2017.11.095
29. Frazzica, A., Freni, A. (2017). Adsorbent working pairs for solar thermal energy storage in buildings. Renewable Energy, 110, 87–94. doi: https://doi.org/10.1016/j.renene.2016.09.047

30. Koukou, M. K., Vrachopoulos, M. Gr., Tachos, N. S., Dogkas, G., Lymperis, K., Stathopoulos, V. (2018). Experimental and computational investigation of a latent heat energy storage system with a staggered heat exchanger for various phase change materials. Thermal Science and Engineering Progress, 7, 87–98. doi: https://doi.org/10.1016/j.tsep.2018.05.004
31. Jeon, J., Park, J. H., Wi, S., Yang, S., Ok, Y. S., Kim, S. (2019). Latent heat storage biocomposites of phase change material-biochar as feasible eco-friendly building materials. Environmental Research, 172, 637–648. doi: https://doi.org/10.1016/j.envres.2019.01.058 Utelbaeva, A. B., Ermakhanov, M. N., Zhanabai, N. Zh., Utelbaev, B. T., Mel'deshov, A. A. (2013). Hydrogenation of benzene in the presence of ruthenium on a modified montmorillonite support. Russian Journal of Physical Chemistry A, 87 (9), 1478–1481. doi: https://doi.org/10.1134/s0036024413090276
32. Borodin, K., Zhangabayuly Zhangabay, N. (2019). Mechanical characteristics, as well as physical-and-chemical properties of the slag-filled concretes, and investigation of the predictive power of the metaheuristic approach. Curved and Layered Structures, 6 (1), 236–244. doi: https://doi.org/10.1515/cls-2019-0020
33. Qiu, F., Song, S., Li, D., Liu, Y., Wang, Y., Dong, L. (2020). Experimental investigation on improvement of latent heat and thermal conductivity of shape-stable phase-change materials using modified fly ash. Journal of Cleaner Production, 246, 118952. doi: https://doi.org/10.1016/j.jclepro.2019.118952
34. Sarsenbaev, A. A. et al. (2019). Pat. No. 4426 RK. Konstrukciya ograzhdeniya s energoaktivnoy panel'yu. No. 2019/0614.2; declareted: 02.07.2019; published: 08.11.2019. Available at: https://gosreestr.kazpatent.kz/Utilitymodel/Details?docNumber=315556
35. Shandilya, A., Hauer, M., Streicher, W. (2020). Optimization of Thermal Behavior and Energy Efficiency of a Residential House Using Energy Retrofitting in Different Climates. Civil Engineering and Architecture, 8 (3), 335–349. doi: https://doi.org/10.13189/cea.2020.080318
36. Saparov, S. A. et al. (2019). Pat. No. 34970 RK. Teploakkumuliruyushchiy material. No. 2019/0897.1; declareted: 10.12.2019; published: 11.06.2021. Available at: https://gosreestr.kazpatent.kz/Invention/Details?docNumber=321931
37. Ikutegbe, C. A., Farid, M. M. (2020). Application of phase change material foam composites in the built environment: A critical review. Renewable and Sustainable Energy Reviews, 131, 110008. doi: https://doi.org/10.1016/j.rser.2020.110008
38. Duissenbekov, B., Tokmuratov, A., Zhangabay, N., Orazbayev, Z., Yerimbetov, B., Aldiyarov, Z. (2020). Finite-difference equations of quasistatic motion of the shallow concrete shells in nonlinear setting. Curved and Layered Structures, 7 (1), 48–55. doi: https://doi.org/10.1515/cls-2020-0005
39. Yao, C., Kong, X., Li, Y., Du, Y., Qi, C. (2018). Numerical and experimental research of cold storage for a novel expanded perlite-based shape-stabilized phase change material wallboard used in building. Energy Conversion and Management, 155, 20–31. doi: https://doi.org/10.1016/j.enconman.2017.10.052
40. James, C., Yuen-Yick, K. (2009). A brief review of several numerical methods for one-dimensional Stefan problems. Thermal Science, 13 (2), 61–72. doi: https://doi.org/10.2298/tsci0902061c
41. Samarskij, A. A., Vabishchevich, P. N. (2003). Vychislitel'naya teploperedacha. Moscow: Editorial URSS, 784. Available at: http://samarskii.ru/books/book2003.pdf
42. 2009 ASHRAE Handbook – Fundamentals (SI Edition). Available at: https://www.pdfdrive.com/2009-ashrae-handbook-fundamentals-si-edition-e169690158.html
43. Kutateladze, S. S. (1990). Teploperedacha i gidrodinamicheskoe soprotivlenie. Moscow: Energoatomizdat, 367.
44. Aymbetova, I. O., Suleymenov, U. S., Kambarov, M. A., Kalshabekova, E. N., Ristavletov, R. A. (2018). Thermophysical properties of phase transparent heat-storing materials used in construction. Advances in Current Natural Sciences, 1 (12), 9–13. doi: https://doi.org/10.17513/use.36966